Recibido: 16/09/2024
Aceptado: 03/12/2024
Disponible en línea: 13/01/2025
Publicado: 31/01/2025

REVISTA DE TELEDETECCIÓN
Asociación Española de Teledetección
(2025) 65, 22317
ISSN 1133-0953
EISSN 1988-8740
https://doi.org/10.4995/raet.2025.22317

Using satellite imagery to assess glacier retreat in King George Island, Antarctica

Ibeth Rojas-Macedo [1,2*], Cinthya Bello [3], Wilson Suarez [4], Edwin Loarte [5], Fiorella Vega-Jacome [6], Maria G. Bustamante Rosell [1], Pedro M. Tapia [7]

[1] *National Institute of Glaciers and Mountain Ecosystems of Peru/INAIGEM, Av. Centenario 2656, Huaraz, Ancash, Perú.*

[2] *National Agrarian University La Molina /UNALM, Master in Water Resources/MRH, Lima, Peru.*

[3] *Carrera de Biología Marina, Universidad Científica del Sur, Panamericana Sur km 19, Villa El Salvador, Perú.*

[4] *Meteorological and Hydrological Service of Peru, Jr. Cahuide 721, Lima, Perú.*

[5] *Research Center for Environmental Earth Science and Technology (ESAT), Santiago Antúnez de Mayolo National University (UNASAM), Huaraz, Perú.*

[6] *Institute of Environmental Science and Geography, University of Potsdam, Potsdam, Germany.*

[7] *Universidad Peruana Cayetano Heredia, Av. Honorio Delgado 430, San Martin de Porres, Perú.*

Abstract: In recent decades, remote sensing has become a powerful tool for continuously monitoring glacier dynamics in remote areas, enabling the identification of significant spatiotemporal changes due to its capacity to provide multitemporal information at regional and global scales. In this study, Landsat satellite images (1989–2020) were used to quantify glacier retreat in the ice cap of King George Island (KGI), located in the Antarctic Peninsula, and to evaluate the teleconnections of El Niño – Southern Oscillation - ENSO (ONI and SOI indices) with climatic variables (temperature and precipitation) in this region. Our findings reveal a 10% loss in glacier coverage over the last 31 years, with a slower glacier retreat observed since 2008. Glaciers with smaller areas and marine terminating were the most affected. Of the 73 glaciers on KGI, 42% had continental terminating, 21% had marine terminating, and 37% had mixed terminating (continental and marine). Of the total glacier area lost, 35% corresponds to glaciers with marine terminating, while 16% corresponds to glaciers with continental terminating. Furthermore, climatic variables exhibited heterogeneous responses during ENSO events, with a significant correlation between mean temperature and ONI at the annual level and during the austral spring, which may be influencing glacier retreat in the study area to some extent.

Key words: remote sensing, King George Island, glacier retreat, El Niño-Southern Oscillation, Antarctica.

Utilización de imágenes por satélite para evaluar el retroceso de los glaciares en la Isla Rey Jorge (Antártida)

Resumen: En las últimas décadas, la teledetección ha representado una poderosa herramienta para monitorear continuamente la dinámica de los glaciares en áreas remotas, permitiendo identificar cambios espacio-temporales significativos debido a su capacidad de proporcionar información multitemporal a escalas regional y global. En este estudio se utilizaron imágenes de satélite Landsat (1989-2020) para cuantificar el retroceso de los glaciares en la capa de hielo de la Isla Rey Jorge (KGI), en la Península Antártida y evaluar las teleconexiones de El Niño- Oscilación del Sur - ENOS (índices ONI y SOI) con las variables climáticas (temperatura y precipitación) en esta región.

To cite this article: Rojas-Macedo, I., Bello, C., Suarez, W., Loarte, E., Vega-Jacome, F., Bustamante-Rosell, M.G., Tapia, P.M. 2025. Using satellite imagery to assess glacier retreat in King George Island, Antarctica. *Revista de Teledetección*, *65*, 22317. https://doi.org/10.4995/raet.2025.22317

* *Corresponding author: ibeth.rojas@icloud.com*

Nuestros hallazgos revelan que se perdió 10% de cobertura glaciar en los últimos 31 años, evidenciándose una menor recesión glaciar a partir del 2008; siendo principalmente los glaciares con menor área y con terminaciones marinas los más afectados. Además, de los 73 glaciares en KGI, el 42% tenía terminación continental; el 21%, terminación marina; y el 37%, terminación mixta (continental y marina). Del total del área glaciar perdida, el 35% corresponde a los glaciares con terminación marina y un 16%, a glaciares de terminación continental. Por otro lado, las variables climáticas mostraron una respuesta heterogénea durante los eventos ENSO, resaltando la correlación significativa entre la temperatura promedio y el ONI a nivel anual y durante la primavera austral, lo cual podría estar influenciando en alguna medida en el retroceso glaciar en la zona de estudio.

Palabras clave: Isla Rey Jorge, retroceso glaciar, El Niño-Oscilación del Sur, Antártida.

1. Introduction

Global warming triggers shrinking and thinning of glaciers worldwide, with potentially severe implications (Yao-Jun *et al.*, 2019; Paolo *et al.*, 2018; Berthier *et al.*, 2023; Rückamp *et al.*, 2011). Since the industrial revolution, polar regions have doubled their average temperature (Siegert *et al.*, 2019)and clear cryospheric and biological consequences have been observed. Under a global 1.5°C scenario, warming in the Antarctic Peninsula is likely to increase the number of days above 0°C, with up to 130 of such days each year in the northern Peninsula. Ocean turbulence will increase, making the circumpolar deep water (CDW; therefore, they are losing ice, and their oceans are changing rapidly with consequences for the whole planet. Yuan (2004) stated that the cryosphere of the Southern high latitudes influences climate regulation on a global scale. Antarctica exhibits marked regional differences in glacier retreat rate, which could be connected with climatic forcing (Meredith & King, 2005, Yao-Jun *et al.*, 2019), in particular with the Southern Annual Mode (SAM) and El Niño-Southern Oscillation (ENSO) (Clem *et al.*, 2016). Some researchers suggested that the Antarctic sea ice fields linearly co-vary with the El Niño/Southern Oscillation (ENSO) phenomenon by tropical Pacific (Yuan, 2004); Kwok & Comiso (2002) note that a weak negative sea temperature anomaly near the Antarctic Peninsula region is actually associated with ENSO episodes. In addition, Paolo *et al.* (2018) affirms that during intense El Niño years net ice-shelf mass declines as basal ice loss exceeds ice gain by lower-density snow. In Antarctica, the South Shetland Islands (SSI) were subject to strong warming trends in the atmospheric surface layer. Surface air temperature increased by about 3 °K in 50 years, concurrent with retreating glacier fronts, an increase in melt areas, ice surface lowering, and rapid break-up and disintegration of ice shelves (Falk *et al.*, 2018).

In recent decades, glaciological and geodetic methods have been used to monitor glaciers worldwide (Berthier *et al.*, 2023; Cogley, 2009; Zemp & Welty, 2023; Fischer, 2011).

Nevertheless, since the beginning of the satellite era geodetic methods have been widely used to monitor glaciers located in remote areas, difficult to access, and with great glacial extension, such as Antarctica (Bolch *et al.*, 2010; Rastner *et al.*, 2012,; Rajat *et al.*, 2022; Miles & Bingham, 2024). Remote sensing have been used for glacier delineation, encompassing passive optical sensors, active microwave sensors like synthetic aperture radars (SAR), and active altimetry sensors (Marghany, 2016). Optical sensor products such as Landsat and ASTER, with long temporal record, starting from the 1970s, offer medium spatial resolution in multispectral mode with wide swath coverage and relatively short revisit times, making them well-suited for extensive and regular glacier mapping (Racoviteanu *et al.*, 2008). However, optical sensors are limited by atmospheric interference, particularly in polar regions with frequent cloud cover (Gabarró *et al.*, 2023). SAR products like Sentinel-1 overcome these atmospheric constraints due to their ability to penetrate cloud cover and operate in day and night conditions (European Space Agency, 2013). However, their data records are relatively recent, beginning around 2015, which restricts their application for long-term analyses. This limitation highlights the continued value of Landsat data for glacier mapping and the assessment of temporal variations in response to climate change (Ali *et al.*, 2023). Between the numerous methods for

multispectral glacier delineation (Kääb, 2005), manual digitization, done by a glaciologist experienced in studying glaciers in remote sensing imagery, can achieve the highest accuracy compared with computer algorithms (Kääb, 2005; Raup *et al.*, 2014), particularly efficient in relatively small glaciers.

King George Island (KGI) presents land-terminating and marine-terminating glaciers (Da Rosa *et al.*, 2020; Cook *et al.*, 2014). Simões *et al.* (1999) found that glacier fronts at KGI, Antarctic Peninsula receded 7% (89 km^2) between 1956-1995. Rückamp *et al.* (2011) determined that the strongest area loss for the period 2000-2008 was recorded in marine-terminating glaciers draining into King George Bay. Liang *et al.* (2019) affirmed that marine-terminating and land-terminating glaciers in the Antarctic region are both important targets for comprehending the glacier responses and sensitivity to changes in climate. Da Rosa *et al.* (2020) considered glacier geomorphological changes as environmental fluctuations indicators. Nevertheless, Lee *et al.* (2008) affirm that marine-terminating glaciers are more important because such sea-contact glaciers are more sensitive than land glacier to the climate changes. Ma & Bassis (2019) affirm that glacier retreat associated with marine-terminating glaciers is more sensitive to submarine melting and glacier calving. This study aims to evaluate the teleconnections between ENSO events and climatic variables on King George Island (KGI) and to quantify glacier retreat across its ice cap using Landsat satellite images.

2. Materials and Methods

2.1. Study area

KGI (Figure 1) is the largest of the South Shetland Islands, located 130 km at the northwestern tip of the Antarctic Peninsula (AP) (Falk *et al.*, 2018), between 57° 35' and 59° 02' W, 61° 54' and 62° 16' S, with a length and width approximately of 79 and 27 km, respectively (Simões *et al.*, 1999). About 90 % of the KGI is ice-covered (Simões *et al.*, 1999), and influenced by maritime

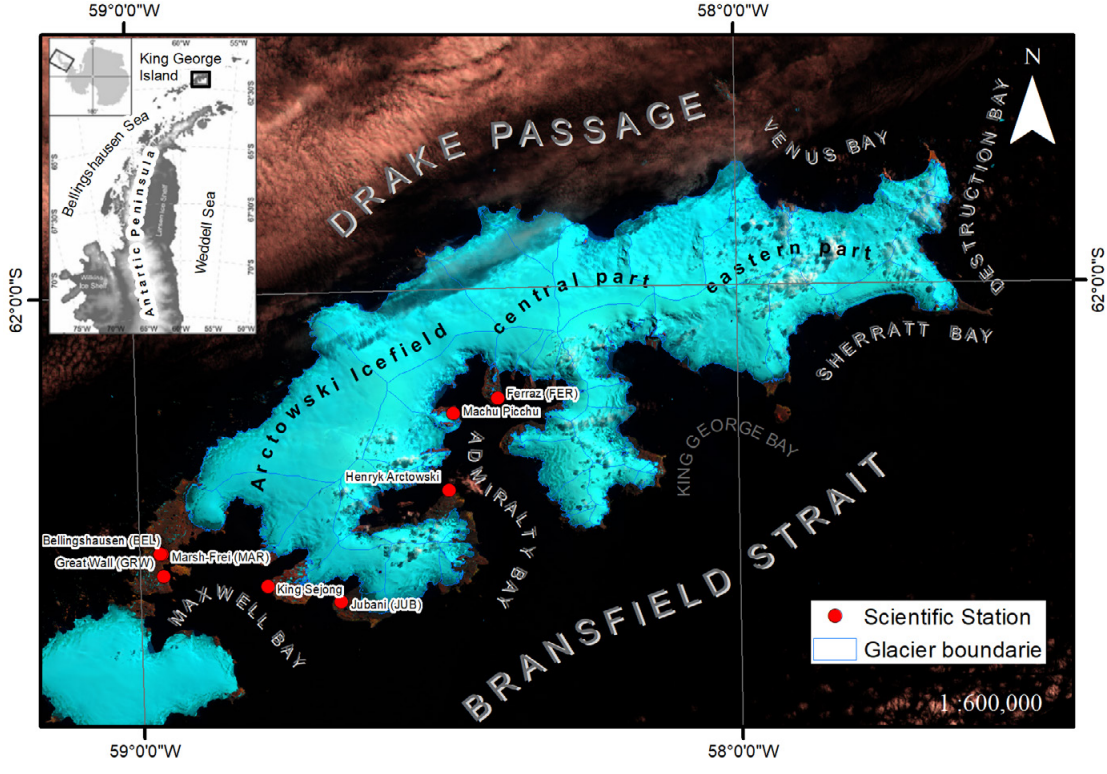

Figure 1. King George Island location.

climatic conditions (Falk *et al.*, 2018; Rückamp & Blindow, 2012; Ferron *et al.*, 2004), with land-terminating and marine-terminating glaciers whose altitude varies between 0 to 700 m a.s.l. The average air temperature registered at Peninsula Fildes (Simões *et al.*, 1999) was -2.8°C between 1947-1995, while at KGI was -2.5°C for the period 1948-2011 (Kejna *et al.*, 2013). Temperatures rise above freezing in summer, and regularly during the spring and autumn months causing snowmelt. However, during the winter surface snowmelt is also observed occasionally (Rückamp *et al.*, 2011).

2.2. Climatic data

Surface air temperature (2 m) monthly data from five stations located on KGI were used. The data series of the stations Bellingshausen (BEL), Jubany (JUB), and Great Wall (GRW) were obtained from the SCAR READER database available at https://legacy.bas.ac.uk/met/READER/surface/stationpt.html. Meanwhile, the data from Marsh or Frei (MAR) and Ferraz (FER) stations were downloaded from https://climatologia.meteochile.gob.cl/application/historicos/datosDescarga/950001 and http://antartica.cptec.inpe.br/, respectively. Monthly precipitation data series for Bellingshausen and Marsh stations were obtained from http://www.aari.aq/data/data.php?lang=1&station=0 and https://climatologia.meteochile.gob.cl/application/historicos/datosDescarga/9500, respectively (Table 1). We organized the data in glaciological years, where the glaciological year n is defined from September (year n) to August (year n+1). Seasonal periods were organized as follows: spring (September, October, and November -SON); summer (December, January, and February -DJF); autumn (March, April, and May -MAM); and winter (June, July, and August -JJA). The climatic variables were analysed for the period from 1980 to 2019. The temporal temperature series had less than 15 % of missing data and were well correlated between stations, for this reason the missing data of each station was completed by linear regressions with the regional vector. In case of precipitation series, the missing data was completed using linear regression between stations.

2.3. Teleconnection analysis

We used oceanic and atmospheric circulation indices to measure the influence of the ENSO variability: 1) Oceanic Niño Index (ONI) (available at https://psl.noaa.gov/data/correlation/oni.data), ONI is the running mean anomalies of three consecutive months of the Sea Surface Temperature (SST) in the region 3.4 of El Nino, and 2) Southern Oscillation Index (SOI) (available at https://psl.noaa.gov/data/correlation/soi.data), the SOI is one measure of the large-scale fluctuations in air pressure occurring between the western and eastern tropical Pacific during El Niño and La Niña episodes. These indices were selected based on previous research work that studied the influence of ONI (Walker & Gardner, 2017 and Paolo *et al.*, 2018) and SOI (Clem & Fogt, 2013; Clem *et al.*, 2016 and Santamaría-del-Ángel *et al.*, 2021) on the climatic variability and glacier dynamic in the Antarctic. The indices were classified in 4 ranges to identify ENSO phases (Table 2). The teleconnection was analysed for the period from 1980 to 2019. We used the Pearson correlation coefficient at 95 % significance to identify the relationship between climatic variables and the indices. Subsequently, climate variables were normalized subtracting the mean and dividing by

Table 1. Meteorological stations, where P indicates precipitation and T air temperature.

Station	Code	Country	Variable	Data period	Latitude	Longitude	Altitude (m a.s.l)
Bellingshausen	BEL	Russia	P and T	1980-2019	62.20° S	58.97° W	16
Marsh (Frei)	MAR	Chile	P and T	1980-2019	62.20° S	58.96° W	10
Jubany	JUB	Argentina	T	1980-2019	62.24° S	58.67° W	4
Ferraz	FER	Brazil	T	1980-2019	62.08° S	<58.39° W	20
Great Wall	GRW	China	T	1980-2019	62.22° S	58.96° W	10

Table 2. Variation ranges of ocean-atmospheric indices.

Intensity		
ONI	SOI	ENSO Phase
>0.5	<-0.7	Warm (El Niño)
[0;0.5]	[-0.7;0]	Neutral Warm
[-0.5 ; 0]	[0;0.7]	Neutral Cold
<-0.5	>0.7	Cold (La Niña)

the standard deviation, and organized in ascending order of the indices to identify ENSO events influence.

2.4. Glacier delimitation

Landsat satellite images (4-5, 7, and 8) with a spatial resolution of 30 m were used (Table 3) for the delimitation of glacier coverage. These images were downloaded from the GLOVIS portal of the United States Geological Survey (USGS), available at https://glovis.usgs.gov/app?fullscreen=0.

To select the multitemporal images, we prioritized those with minimal to no cloud cover over KGI, excluding images from winter months (June, July, and August) to avoid interference from seasonal snow cover that could disturb the identification of glacier front displacement. It was used Landsat Tier 2 images (good quality), accurate for land cover classification.

Glacier coverage in KGI was made through manual delimitation (Marghany, 2016; Baumhoer *et al.*, 2018). The GLIMS Classification (Global Land Ice Measurements from Space) version 6 (RGI Consortium, 2017) was used to discriminate the glacier units in KGI. GLIMS Classification was spatially adjusted based on a TanDEM-X Digital Elevation Model (2016) with a spatial resolution of 90 m, available at https://geoservice.dlr.de/web/dataguide/tdm90/. The resulted adjusted GLIMS shapefile was overlapped with the temporal manual delimitation of the glacier fronts in KGI.

3. Results

3.1. Climatic variables and ENSO teleconection

Table 4 shows the average air temperature and precipitation for the stations analysed in the study area. The mean temperatures for the complete period range from -5.6 °C to 1.8 °C, while the precipitation varies from 130.8 mm to 704.8 mm. The mean temperature between December and March was above 0°C, reaching up to 1.8°C (FER), with February being the warmest month of the year. Between April and November, the temperature was below 0°C, with temperatures that reached -5.6 °C (BEL).

The Table 5 shows the teleconnection analysis, where the annual and seasonal (SON) temperatures at the five weather stations are correlated negatively and significantly with the ONI. This means that air temperatures on KGI are higher during negative SST anomalies in the central Pacific. However, the behaviour was opposite (positive correlation)

Table 3. List of satellite images of King George Island, with their GLOVIS server code.

Year	Sensor Type	Spatial Resolution (m.)	Satellite Image (server code)
1989	TM (Landsat 4)	30	LT04_L1GS_217103_19890128_20170204_01_T2
2001	ETM+ (Landsat 7)	30	LE07_L1GS_218103_20011206_20170202_01_T2
2005	ETM+ (Landsat 7)	30	LE07_L1GS_217103_20050209_20170116_01_T2
2007	ETM+ (Landsat 7)	30	LE07_L1GS_217103_20070114_20170105_01_T2
2008	ETM+ (Landsat 7)	30	LE07_L1GS_217103_20080117_20161231_01_T2
2014	OLI/TIRS (Landsat 8)	30	LC08_L1GT_218103_20140116_20170426_01_T2
2015	OLI/TIRS (Landsat 8)	30	LC08_L1GT_218103_20150425_20170409_01_T2
2016	OLI/TIRS (Landsat 8)	30	LC08_L1GT_217103_20161029_20170319_01_T2
2017	OLI/TIRS (Landsat 8)	30	LC08_L1GT_217103_20170306_20170316_01_T2
2020	OLI/TIRS (Landsat 8)	30	LC08_L1GT_216104_20200119_20200128_01_T2

Table 4. Climatological average of air temperature and precipitation for the period 1980-2019, the values in parentheses indicate the standard deviation.

	T (°C)					P (mm)				
Station	Annual	SON	DJF	MAM	JJA	Annual	SON	DJF	MAM	JJA
BEL	-2.2 (0.6)	-2.7 (1.0)	1.1 (0.6)	-1.5 (1.0)	-5.6 (1.8)	704.8 (108.3)	167.3 (56.0)	168.3 (34.3)	195 (43.5)	174.2 (66.8)
MAR	-2.2 (0.6)	-2.8 (0.9)	1.0 (0.6)	-1.6 (0.9)	-5.6 (1.7)	561.7 (201.8)	149.6 (93.7)	130.8 (36.2)	148.9 (64.3)	132.3 (94.9)
FER	-1.7 (0.7)	-2.1 (1.1)	1.8 (0.7)	-1.1 (1.1)	-5.4 (1.9)	-	-	-	-	-
JUB	-1.8 (0.6)	-2.2 (1.0)	1.7 (0.5)	-1.2 (1.2)	-5.4 (1.8)	-	-	-	-	-
GRW	-2.1 (0.6)	-2.7 (0.9)	1.4 (0.5)	-1.5 (1.0)	-5.6 (1.7)	-	-	-	-	-

with the SOI. For the precipitation, only the BEL station showed a significant negative (positive) correlation during the annual and SON period with the ONI (SOI).

For the air temperature, MAR station showed a negative correlation during the annual period (-0.36) and SON (-0.39) with the ONI index. While SON register an opposite behaviour (0.31) with the SOI index. BEL station showed a negative correlation during the annual period and SON with a value up to -0.4 for the ONI index. However, positive correlations were found for the annual period (0.32) and SON (0.35) with the SOI index. FER station registered a negative (positive) correlation at annual scale and spring season up to -0.41 (0.31) and -0.46 (0.37) with the ONI (SOI) index. JUB station showed a negative correlation with the ONI index for the annual period and SON with values up to -0.41 and -0.42 respectively. These same periods exhibited a positive correlation with values of 0.34 (annual) and 0.37 (SON) with the SOI index. Like previous stations, GRW presented a negative correlation with the ONI index for the annual period (-0.38) and SON (-0.38), and a positive correlation with the SOI index for the annual period (0.29) and spring season (0.34).

For the precipitation, BEL station shows significant correlations with the ENSO indices. Specifically, a negative correlation for the ONI index at the annual scale (-0.43) and SON (-0.39), while the SOI index registers an opposite behaviour for both periods with a value up to 0.30. However, MAR station does not show significant correlations.

Table 6 shows the relationship between the ONI and SOI with the climatic variables (surface air temperature and precipitation) to characterize the ENSO events. The surface air temperature

Table 5. Pearson correlation at 95% confidence, between air temperature and precipitation for ONI and SOI, values in bold italics are significant.

		ONI					SOI				
Variable	Station	SON	DJF	MAM	JJA	Annual	SON	DJF	MAM	JJA	Annual
T	MAR	***-0.39***	-0.14	-0.07	-0.19	***-0.36***	***0.31***	-0.03	0.11	0.15	0.23
	BEL	***-0.40***	-0.20	-0.12	-0.20	***-0.40***	***0.35***	0.08	0.15	0.15	***0.32***
	FER	***-0.46***	-0.22	-0.05	-0.16	***-0.41***	***0.37***	0.14	0.11	0.12	***0.31***
	JUB	***-0.42***	-0.27	-0.12	-0.19	***-0.41***	***0.37***	0.17	0.14	0.15	***0.34***
	GRW	***-0.38***	-0.25	-0.11	-0.19	***-0.38***	***0.34***	0.14	0.11	0.16	***0.29***
P	MAR	-0.17	-0.01	0.03	0.11	0.02	0.08	-0.13	0.02	-0.01	-0.19
	BEL	***-0.39***	-0.20	-0.06	0.20	***-0.43***	***0.30***	0.05	0.10	-0.22	***0.33***

Table 6. Variability of precipitation and temperature in normalized values during different phases of ONI and SOI index, red color indicates variations above 0.5 standard deviations, pink color indicates variations between 0.5 and 0, light blue color indicates variations between 0 to -0.5 and turquoise color indicates variations below -0.5.

	Variable	Station	ONI				SOI			
			<-0.5 (cold phase)	[-0.5_0]	[0_0.5]	>0.5 (warm phase)	<-0.7 (warm phase)	[-0.7_0]	[0_0.7]	>0.7 (cold phase)
Annual	T	BEL	0.71	0.00	-0.16	-0.46	-0.36	-0.26	0.15	0.43
		MAR	0.66	-0.05	-0.11	-0.42	-0.27	-0.22	0.16	0.22
		FER	0.84	-0.08	-0.21	-0.40	-0.32	-0.26	0.11	0.44
		JUB	0.69	0.14	-0.23	-0.49	-0.36	-0.35	0.21	0.42
		GRW	0.69	0.07	-0.24	-0.40	-0.31	-0.34	0.20	0.38
	P	BEL	-0.32	0.31	0.07	-0.18	-0.12	-0.04	0.12	0.01
		MAR	-0.25	0.31	-0.25	0.28	0.17	-0.42	0.56	-0.50
SON	T	BEL	0.13	0.83	-0.44	-0.53	-0.45	-0.04	0.37	0.20
		MAR	0.07	0.86	-0.38	-0.53	-0.46	0.12	0.35	0.12
		FER	0.15	0.86	-0.48	-0.56	-0.45	-0.06	0.32	0.26
		JUB	0.14	0.82	-0.39	-0.56	-0.51	-0.04	0.42	0.21
		GRW	0.10	0.85	-0.34	-0.57	-0.51	-0.02	0.47	0.16
	P	BEL	0.35	0.12	-0.21	-0.33	-0.32	-0.21	0.12	0.41
		MAR	0.10	0.01	0.24	-0.23	0.06	0.01	-0.11	0.03
DJF	T	BEL	0.28	-0.21	0.14	-0.2	0.06	-0.4	0.08	0.09
		MAR	0.16	-0.19	0.53	-0.25	0.12	-0.59	0.33	-0.15
		FER	0.34	-0.24	-0.36	-0.05	0.02	-0.19	-0.03	0.13
		JUB	0.38	-0.12	-0.06	-0.28	-0.11	-0.21	0.12	0.15
		GRW	0.27	0.03	-0.03	-0.27	-0.11	-0.04	0.03	0.18
	P	BEL	-0.04	0.01	0.59	-0.19	0.1	-0.87	0.31	-0.03
		MAR	-0.22	0.28	0.73	-0.23	-0.06	-0.43	0.82	-0.52

for all the stations shows that, at annual scale the cold phase (La Niña) of the ONI index increases significantly, exceeding the limit value. However, during the warm phase (El Niño) the ONI index shows an opposite behaviour, with the index decreasing. During SON (spring), the ONI and SOI index in the cold phase (La Niña) show an increase in surface air temperature. During the warm phase (El Niño), a temperature decrease is observed with values below -0.53 and -0.45 for the ONI and SOI index. In DJF, the cold phase for both indices show an increase in air surface temperature except for MAR station in SOI. Moreover, all the stations show a decrease registered in the ONI warm phase. A similar pattern was recorded with the SOI warm phase for JUB and GRW stations.

For the precipitation, only BEL had significant correlations with the ENSO indices. In the annual period, for the ONI cold phase, the precipitation decreases in BEL and MAR, which is not significant for the SOI cold phase. In the warm phase, BEL shows that precipitation decreases with ONI (-0.18) and SOI (-0.12). During SON the cold phase for both indices registered an increase in precipitation. Likewise, in DJF during the SOI cold phase, the precipitation decreases in both stations (BEL and MAR). Concerning the

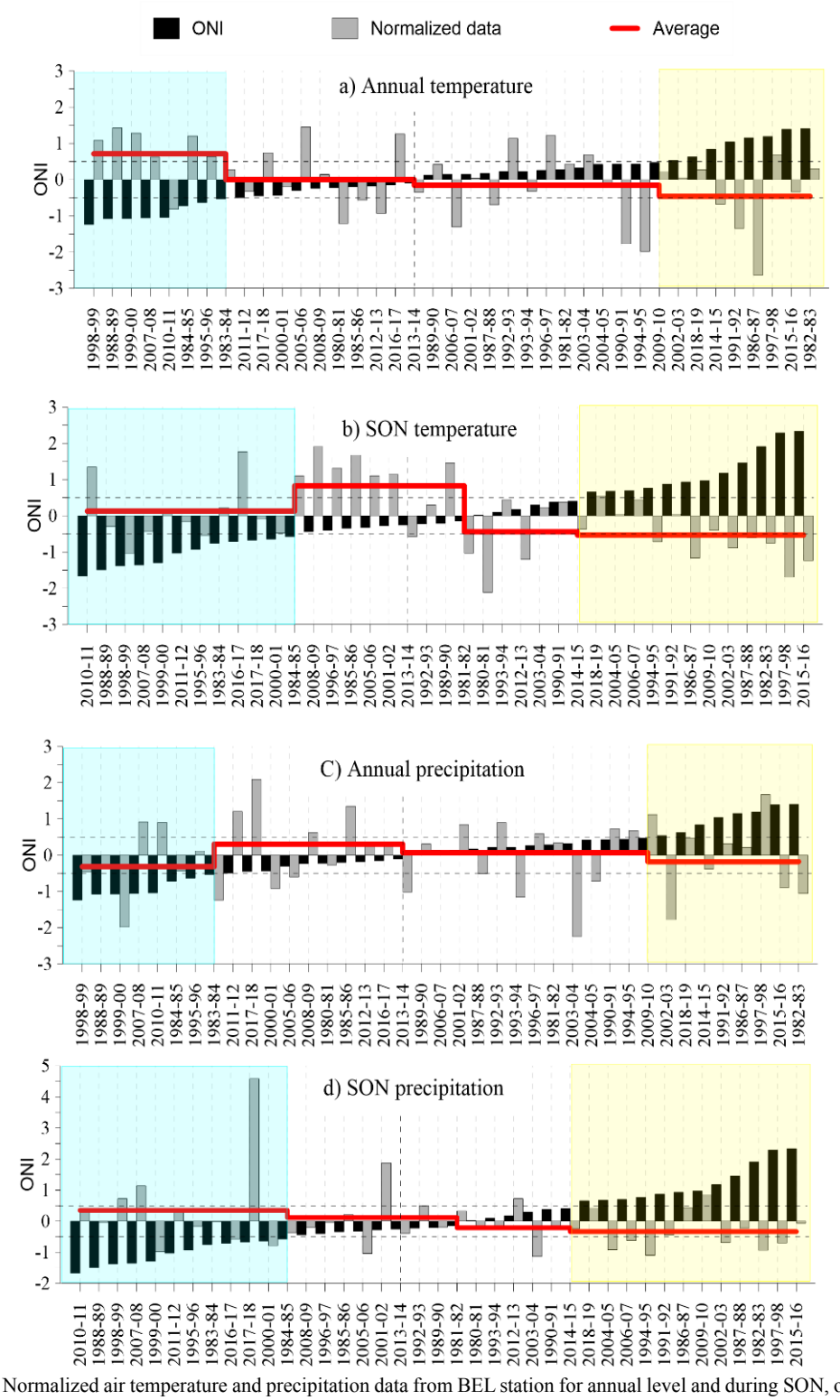

Figure 2. Normalized air temperature and precipitation data from BEL station for annual level and during SON, ordered according to increasing ONI pattern. Shaded in turquoise and yellow areas represent cold (La Niña) and warm phase (El Niño), respectively. Green lines represent the average value (precipitation or temperature) recorded according to ONI intensity.

BEL station, the warm phase shows an opposite behaviour for the ONI and SOI.

In order to see the impact during the most characteristic years of both El Niño and La Niña, it is necessary to perform a detailed analysis at the station level. For this analysis, the ONI index and the BEL station were selected considering that the air temperature of BEL station has a similar pattern to the other stations in the study area, while in the case of precipitation, it is the only station that presented significant correlations with the analysed ENSO indices. Figure 2 shows the normalized data of air temperature and precipitation for the Annual and SON period, which are ordered following the increasing pattern of the ONI, likewise, the shaded areas represent in turquoise the cold phase (La Niña) and in yellow the warm phase (El Niño). Figure 2a for the annual temperature shows that out of 39 years analysed, 13 years (~30% of the period) exceeded the threshold of 0.5 standard deviations, which indicates an abnormal increase in temperature in those years, where six of the 13 years occurred within the cold phase and one within the warm phase of the ONI. From these results, we can infer that at annual scale level during La Niña events the temperature is more likely to increase, while during the warm phase, there could be (not always) a decrease in temperature. Figure 2b shows the air temperature for the SON period, in the cold phase two years exceed the threshold of 0.5, and seven years are below 0 (only two below -0.5). Likewise, during the cold phase, the mean (dotted line) is strongly influenced by the increase in temperature recorded in the years 2016-2017 and 2010-2011 but the largest number of events are below 0. During the warm phase, 13 years were recorded, of which four were positive and nine negatives. In the seven years where the ONI signal was stronger, the temperature showed a decrease and six of these years were below the threshold (-0.5), from which it is inferred that a decrease in temperature would be expected in the face of intense El Niño signals. Regarding annual precipitation (Figure 2c and 2d), we find that precipitation behaviour under different phases of ONI is variable with no clear relationships observed between these variables.

3.2. Glacier area changes in KGI

The predominant orientation of the glaciers in the KGI is south, southeast, north, and east, with a slope that varies between the range of 6° to 15°. In 1989, the glacier coverage of KGI was 1098.42 km² distributed among 73 glaciers (Figure 3). However, by 2020 the coverage was reduced to 989.45 km^2; thus, in 31 years, 108.97 km^2 of glacier coverage has been lost, equivalent to a loss of 9.92% of its area with an average retreat rate of 3.52 $km^2 \cdot year^{-1}$ for the study period (Table 7). Also, glacier retreat rates observed during the second half (2007-2015) of the study period show a slight deceleration (0.09 $km^2 \cdot year^{-1}$) compared to the first half (1989-2006, 0.88 $km^2 \cdot year^{-1}$) period. The highest rate of retreat occurred during 2005–2007, followed by 2001–2005. Many of the glaciers with an area of less than 5 km^2 (Figure 4a) located in the southern part of KGI have shown higher recession rates compared with others in the study area. It is important to mention that, five glaciers have shown significant retreat up to 12 km^2 (since 1989) such as Anna glacier (G-01), Polonia Piedmont glacier (G-02),

Table 7. Changes in glacier cover on King George Island, period 1989-2020.

Year	Area (km^2)	Period (years)	Area lost (km^2)	Area loss (%)	Rate of retreat ($km^2 \times year^{-1}$)
1989	1098.42				
2001	1054.88	12	43.54	3.96	3.63
2005	1034.62	4	20.26	1.84	5.06
2007	1018.76	2	15.86	1.44	7.93
2008	1017.45	1	1.31	0.12	1.31
2014	1003.83	6	13.62	1.24	2.27
2015	1000.26	1	3.57	0.33	3.57
2016	999.44	1	0.82	0.07	0.82
2017	997.57	1	1.87	0.17	1.87
2020	989.45	3	8.12	0.74	2.71
Total	-	31	108.97	9.92	3.52

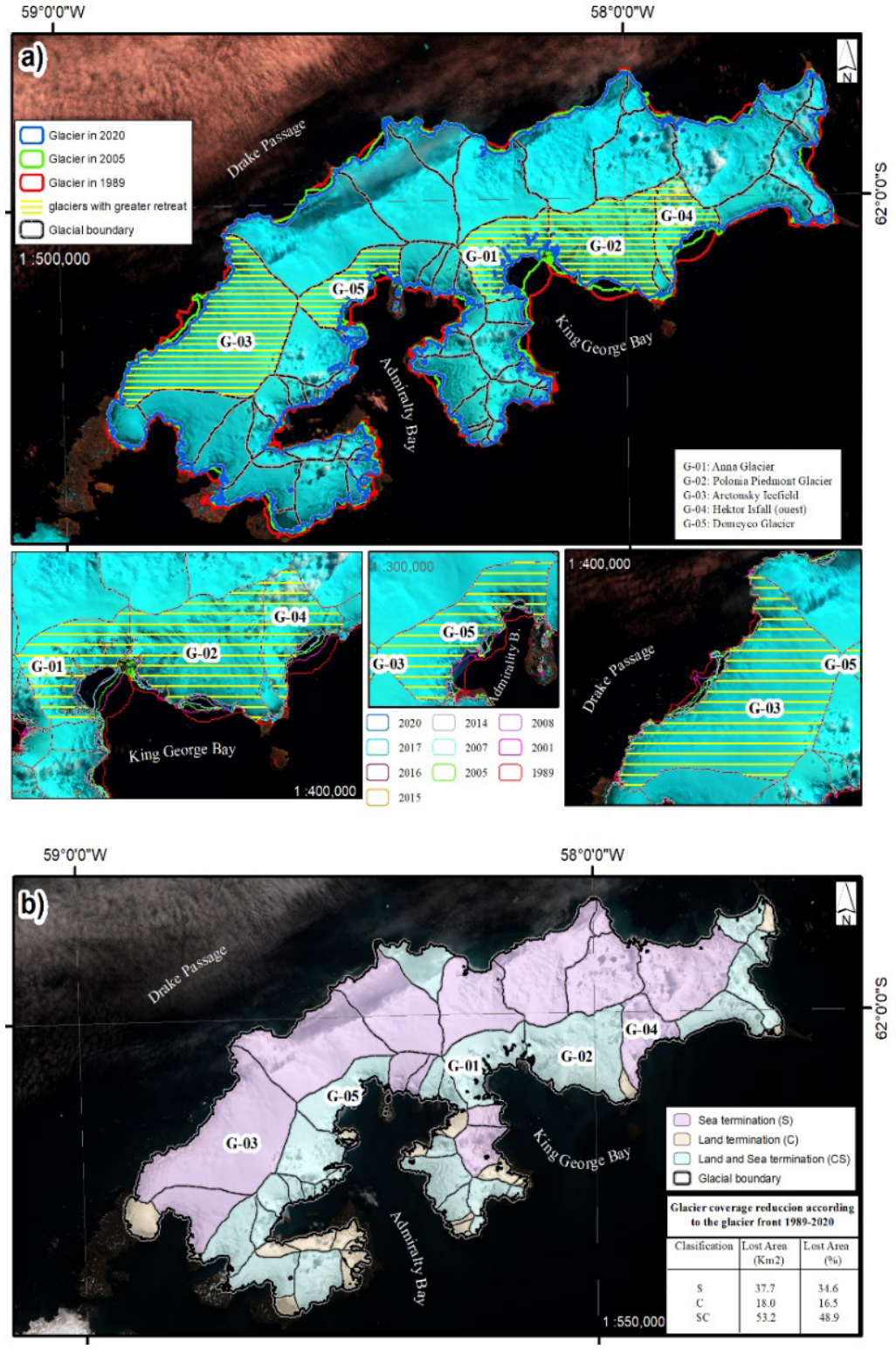

Figure 3. a) Glacier delimitation in KGI specifying the glaciers that have lost more glacier area. b) Map of KGI showing the glaciers according to their frontal termination.

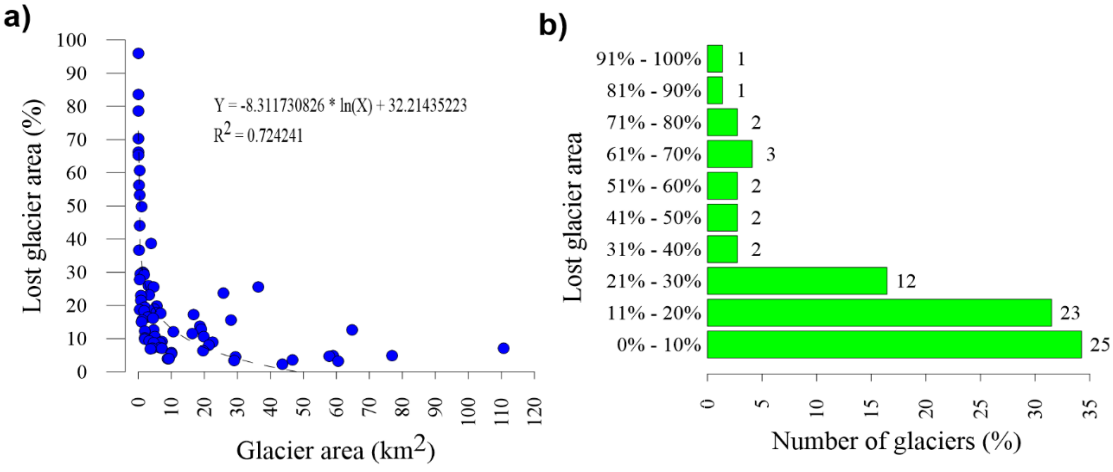

Figure 4. a) Relationship between glacier loss rate and glacier area in 2020, b) glacier loss in percentage related to the number of existing glaciers (the black inner number indicates the number of glaciers).

Arctowski Icefield (G-03), Hektor Isfall Ouest (G-04) and Domeyco glacier (G-05) with 12.5 km^2, 9.36 km^2, 8.43 km^2, 8.0 km^2 and 5.17 km^2 glacier lost, respectively (Figure 3a). In addition, 34% of the glaciers in KGI have lost less than 10% of their glacial area, while 32% of the total glaciers lost between 10% and 20% (Figure 4b). Moreover, of the total of glaciers (73) on KGI, 37% had a mixed terminating, 42% were land-terminating and 21% were marine-terminating. Furthermore, of the total glacier area lost, 35% corresponds to marine-terminating glaciers, 16% corresponds to land-terminating glaciers, and 49% to mixed-terminating glaciers (Figure 3b). In addition, our findings show a recession glacier retreat observed since 2008 (Figure 5).

4. Discussion

In recent decades, some studies (Wei *et al.*, 2019; Santamaría-del-Ángel *et al.*, 2021) have highlighted an asymmetric climate variability between subregions in Antarctica (West Antarctica, East Antarctic, and the Antarctic Peninsula). Our analysis shows that summer temperatures on KGI are above zero between DJF, and near to melting point in SON and MAM. Concerning teleconnections, Pearson coefficient was used to consider the correlation between seasonal and annual surface air temperature, and ENSO index (ONI and SOI). Our results show a Pearson coefficient up to ± 0.4 that coincided with the results obtained by Clem *et al.* (2016) who used the SOI, Niño 3.4, and Southern Annular Mode (SAM) index (1979-2015) observing that

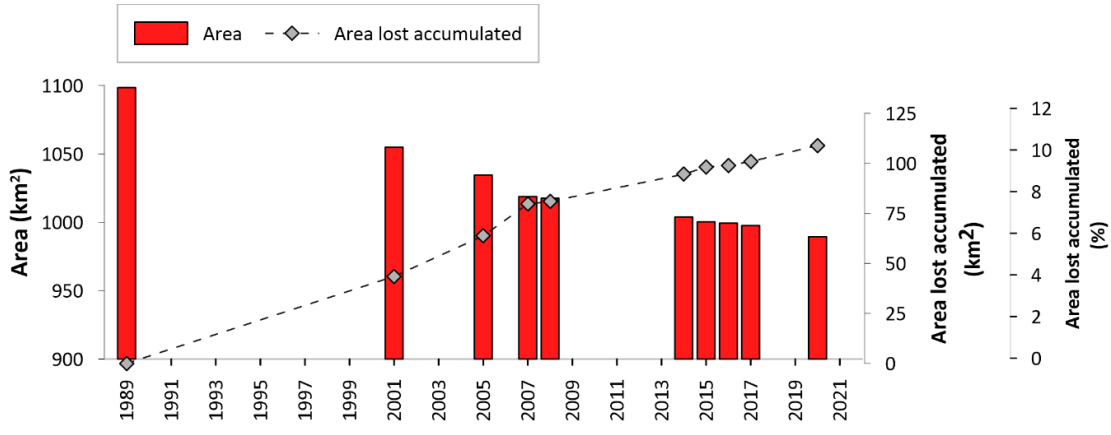

Figure 5. Glacier area and glacier area lost accumulated.

ENSO influence predominates in the Antarctic Peninsula during the austral spring and winter seasons. Several studies affirm that the surface air temperature and precipitation patterns are associated with atmospheric and oceanic warming influenced by SAM and ENSO, impacting different cryosphere components (Turner *et al.*, 2019; Bello *et al.*, 2022). Moreover, several studies have been conducted in KGI to determine changes in some glaciers surface mass balance and frontal position using satellite images and in situ measurements. Our results show that KGI lost 10.3 % (989.5 km^2) of its area, with an average retreat rate of 3.5 $km^2 \cdot year^{-1}$ (Table 7) for the study period (1989-2020), and it is consistent with the findings of other studies. Simões *et al.* (1999) found that the ice cap retreated about 7 % in the period 1956-1995. Rückamp *et al.*, (2011) recorded that KGI lost 20 km^2 (1.6 %) of their total area in nine years (2000-2008). Osmanoğlu *et al.* (2013) confirmed that KGI lost -0.64 ± 0.38 m $w.e.a^{-1}$ between 2008-2011. Sobota *et al.* (2015) identified that Ecology and Sphinx glacial system lost an area of 41 % (1979-2012), a behaviour also observed by Pudełko *et al.* (2018) who registered a retreat of 6.1 km^2 in the eastern part of Warzawa icefield between 1979-2018 (39 years) with a retreat rate that varied depending of the glacier termination, which predominated in marine-terminating glaciers due to the calving effect. In addition, Osmanoğlu *et al.* (2013) showed that both, calving effect and basal melting were the dominant processes in the mass loss in Livingston Island (~120 km west of KGI) from 2007-2011. Moreover, our results show that nearly all marine-terminating and mixed-terminating glaciers are experiencing accelerated changes, with a lost area of up to 91 km^2 (83 %) between 1989-2020. In addition, we find that unlike, the 1982/1983 and 1997/1998 El Niño events, the 2015/2016 El Niño registered values of surface air temperature below the average and a reduction of the precipitation, which could explain the differential glacier retreat. However, a cooling was determined between 2007-2016, associated with a precipitation pattern above the average, which could be associated with the registered recession in KGI in recent years. In the last two decades, the AP has experienced a regional cooling as a result of a decrease in the air surface temperature during the summer months (Carrasco, 2013; Oliva *et al.*, 2017; Turner *et al.*, 2016; Turner *et al.*, 2019; Bello *et al.*, 2022) causing a deceleration in glacial retreat recorded in KGI as in the surrounding islands (Navarro *et al.*, 2013; Osmanoğlu *et al.*, 2013; Marinsek & Ermolin, 2015). Recently, Pętlicki *et al.* (2017) confirmed a deceleration in the ice elevation changes of Ecology glacier between 2012-2016. Fieber *et al.* (2018) determined the elevation and volume change of nine glaciers in KGI, only the Esmerald Icefalls A increased their volume but retreated 70 m between 1956-2013. Kim *et al.* (2021) analysed the glacial dynamics in Marian Cove observing a particular glacial retreat deceleration during 2000-2015 (40 $km \cdot year^{-1}$ with an annual mean temperature of -1.91 °C), compared to the previous period 1989-2000 (64 $km \cdot year^{-1}$ with an annual mean temperature -1.61 °C), similar to the results in the present study. These patterns could explain the glacier retreat rate slowdown for the second half of the present study. Considering that the climate forcing has also been changing since the 1950s, and that the prediction studies indicate that climate warming in the AP will continue over the next decades (Bozkurt *et al.*, 2021), it is very likely that KGI will exhibit volume changes over the next years. Likewise, considering the termination of glaciers in KGI, glaciers with marine termination are more sensitive to marine intrusion generating impacts on the stability of the glacier front, showing radial cracks as a consequence of a progressive process of ice fracture (calving), that accelerated the glacier ice flow. Another element that can contribute to glacial retreat are cryoconites, which are found on glacial surfaces, made up of mineral material (deposited on the ice surface by wind, water and rockfall) and biological material (bacteria, algae and invertebrates), which absorb more solar radiation than the surrounding ice due to their dark color, melting the ice on the glacial surface originating cryoconite holes (Cook *et al.*, 2016).

The spatial variability in the glacial dynamics of KGI, suggest that in addition to atmospheric warming, other factors may influence their dynamics, such as the thermal regime, topography, ocean warming, and radiation exposure (Hock, 2005). Therefore, future observations in surface elevation should confirm these results, especially the influence of the sea-bed topography and water depth over the marine-terminating glaciers.

5. Conclusions

In this study, we use climatic data to determine the influence of ENSO events on the glacier change in KGI between 1980-2019. The teleconnection analysis with indexes (ONI and SOI) showed that climatic variables have great variability and heterogeneous responses during ENSO events. For the surface air temperature, we found significant correlations at the annual level and during the austral spring (SON) with opposite behavior between SOI (positive) and ONI (negative). Likewise, for the studied period (31 years) it was determined 9.92% of glacier recession in KGI. Moreover, of the 73 studied glaciers, 37% have a mixed terminating (land-terminating and marine-terminating), 42% were land-terminating and only 21% were marine-terminating. Furthermore, from total of glacier recession, marine-terminating glaciers had the greatest loss (35%) of ice coverage compared to the land-terminating glaciers (17%). These results show the important implications of calving front processes in the in the displacement of the glacier front. Additionally, we observed that glacier coverage reduction was linked to variations (increase) in annual average air temperature between 1980-2006.

6. Acknowledgements

The present work was financed with the support of the National Fund for Scientific, Technological and Technological Innovation Development of Peru (FONDECYT) 8682-PE with funds from the World Bank and the support of the National Institute of Glaciers and Mountain Ecosystem of Peru (INAIGEM) [Contract No. 003-2018-FONDECYT-BM-IADT-AV], the Office of Antarctic Affairs of the Ministry of Foreign Affairs of Peru (MRE), the National Service of Meteorology and Hydrology of Peru (SENAMHI) and the post-Graduate School in Water Resources of the National Agrarian University La Molina (UNALM). CB was supported by Universidad Científica del Sur (RESOLUCIÓN DIRECTORAL No.008-DGIDI-CIENTIFICA-2024).

References

Ali, A., Dunlop, P., Coleman, S., Kerr, D., Mcnabb, R.W., & Noormets, R. (2023). Glacier area changes in the Arctic and high latitudes using satellite remote sensing. *Journal of Maps*, 1–7. https://doi.org/10.1080/17445647.2023.2247416

Baumhoer, C.A., Dietz, A.J., Dech, S., & Kuenzer, C. (2018). *Remote Sensing of Antarctic Glacier and Ice-Shelf Front Dynamics — A Review*. 1–28. https://doi.org/10.3390/rs10091445

Bello, C., Suarez, W., & Lavado-Casimiro, W. (2022). Trends and space–time patterns of near-surface temperatures on Maxwell Bay, King George Island, Antarctica. *International Journal of Climatology*, *42*(14), 7426–7442. https://doi.org/10.1002/joc.7661

Berthier, E., Floriciou, D., Gardner, A.S., Gourmelen, N., Jakob, L., Paul, F., Treichler, D., Wouters, B., Belart, J.M. C., Dehecq, A., Dussailant, I., Hugonnet, R., Kääb, A., Krieger, L., Pálsson, F., & Zemp, M. (2023). Measuring glacier mass changes from space - a review. *Reports on Progress in Physics*, *86*. https://doi.org/10.1088/1361-6633/acaf8e

Bolch, T., Menounos, B., & Wheate, R. (2010). Remote Sensing of Environment Landsat-based inventory of glaciers in western Canada , 1985 – 2005. *Remote Sensing of Environment*, *114*(1), 127–137. https://doi.org/10.1016/j.rse.2009.08.015

Bozkurt, D., Bromwich, D.H., Carrasco, J., & Rondanelli, R. (2021). Temperature and precipitation projections for the Antarctic Peninsula over the next two decades: contrasting global and regional climate model simulations. *Climate Dynamics*, *56*(11–12), 3853–3874. https://doi.org/10.1007/s00382-021-05667-2

Carrasco, J.F. (2013). Decadal Changes in the Near-Surface Air Temperature in the Western Side of the Antarctic Peninsula. *Atmospheric and Climate Sciences*, *03*(03), 275–281. https://doi.org/10.4236/acs.2013.33029

Clem, K.R., & Fogt, R.L. (2013). Varying roles of ENSO and SAM on the Antarctic Peninsula climate in austral spring. *Journal of Geophysical Research Atmospheres*, *118*(20), 11,481-11,492. https://doi.org/10.1002/jgrd.50860

Clem, K.R., Renwick, J.A., McGregor, J., & Fogt, R.L. (2016). The relative influence of ENSO and SAM on antarctic Peninsula climate. *Journal of Geophysical Research*, *121*(16), 9324–9341. https://doi.org/10.1002/2016JD025305

Cogley, J.G. (2009). Geodetic and direct mass-balance measurements : comparison and joint analysis. *Annals of Glaciology*, *50*(50), 96–100.

Cook, A.J., Vaughan, D.G., Luckman, A.J., & Murray, T. (2014). A new Antarctic Peninsula glacier basin inventory and observed area changes since the 1940s. *Antarctic Science*, *26*(6), 614–624. https://doi.org/10.1017/S0954102014000200

Cook, J. ., Edwards, A., Takeuchi, N., & Irvine-Fynn, T. (2016). Cryoconite: the dark biological secret of the cryosphere. *Progress in Physical Geography*.

Da Rosa, K.K., Perondi, C., Veettil, B.K., Auger, J.D., & Simões, J.C. (2020). Contrasting responses of land-terminating glaciers to recent climate variations in King George Island, Antarctica. *Antarctic Science*, *32*(5), 398–407. https://doi.org/10.1017/S0954102020000279

European Space Agency. (2013). *Sentinel-1 User Handbook Prepared*.

Falk, U., López, D.A., & Silva-Busso, A. (2018). Multi-year analysis of distributed glacier mass balance modelling and equilibrium line altitude on King George Island, Antarctic Peninsula. *Cryosphere*, *12*(4), 1211–1232. https://doi.org/10.5194/tc-12-1211-2018

Ferron, F. a, Simões, J.C., Aquino, F.E., & Setzer, A.W. (2004). Air temperature time series for King George Island, Antarctica. *Pesquisa Antártica Brasileira*.

Fieber, K.D., Mills, J.P., Miller, P.E., Clarke, L., Ireland, L., & Fox, A.J. (2018). Rigorous 3D change determination in Antarctic Peninsula glaciers from stereo WorldView-2 and archival aerial imagery. *Remote Sensing of Environment*, *205*(February 2017), 18–31. https://doi.org/10.1016/j.rse.2017.10.042

Fischer, A. (2011). Comparison of direct and geodetic mass balances on a multi-annual time scale. *Cryosphere*, *5*(1), 107–124. https://doi.org/10.5194/tc-5-107-2011

Gabarró, C., Hughes, N., Wilkinson, J., Bertino, L., Bracher, A., Diehl, T., Dierking, W., Gonzalez-gambau, V., Lavergne, T., Madurell, T., Malnes, E., & Wagner, P.M. (2023). Improving satellite-based monitoring of the polar regions: Identi fi cation of research and capacity gaps. *Frontiers in Remote Sensing*, *February*, 1–15. https://doi.org/10.3389/frsen.2023.952091

Hock, R. (2005). Glacier melt: A review of processes and their modelling. *Progress in Physical Geography*, *29*(3), 362–391. https://doi.org/10.1191/0309133305pp453ra

Kääb, W.R. A. (2005). Remote Sensing of Mountain Glaciers and Permafrost Creep. *Journal of Glaciology*. https://doi.org/10.3189/172756507781833857

Kejna, M., Araźny, A., & Sobota, I. (2013). Climatic change on King George Island in the years 1948-2011. *Polish Polar Research*, *34*(2), 213–235. https://doi.org/10.2478/popore-2013-0004

Kim, D.U., Khim, J.S., & Ahn, I.Y. (2021). Patterns, drivers and implications of ascidian distributions in a rapidly deglaciating fjord, King George Island, West Antarctic Peninsula. *Ecological Indicators*, *125*(January), 107467. https://doi.org/10.1016/j.ecolind.2021.107467

Kwok, R., & Comiso, J.C. (2002). Spatial patterns of variability in Antarctic surface temperature: Connections to the Southern Hemisphere Annular Mode and the Southern Oscillation. *Geophysical Research Letters*, *29*(14), 2–5.

Lee, J., Jin, Y.K., Hong, J.K., Yoo, H.J., & Shon, H. (2008). Simulation of a tidewater glacier evolution in Marian Cove, King George Island, Antarctica. *Geosciences Journal*, *12*(1), 33–39. https://doi.org/10.1007/s12303-008-0005-x

Liang, Q., Zhou, C., Howat, I.M., Jeong, S., Liu, R., & Chen, Y. (2019). Ice flow variations at Polar Record Glacier , East Antarctica. *Journal of Glaciology*, *65*, 279–287. https://doi.org/10.1017/jog.2019.6

Ma, Y., & Bassis, J.N. (2019). The Effect of Submarine Melting on Calving From Marine Terminating Glaciers. *Journal of Geophysical Research: Earth Surface*, *124*(2), 334–346. https://doi.org/10.1029/2018JF004820

Marghany, M. (2016). *Remote Sensing of Mountain Glaciers and Related Hazards*. https://doi.org/10.5772/61917

Marinsek, S., & Ermolin, E. (2015). 10 year mass balance by glaciological and geodetic methods of Glaciar Bahía del Diablo , Vega Island , Antarctic Peninsula. *Annals of Glaciology*, *56*(70), 141–146. https://doi.org/10.3189/2015AoG70A958

Meredith, M.P., & King, J.C. (2005). Rapid climate change in the ocean west of the Antarctic Peninsula during the second half of the 20th century. *Geophysical Research Letters*, *32*(19), n/a-n/a. https://doi.org/10.1029/2005GL024042

Miles, B.W. J., & Bingham, R.G. (2024). Progressive unanchoring of Antarctic ice shelves since 1973. *Nature*, *626*. https://doi.org/10.1038/s41586-024-07049-0

Navarro, F.J., Jonsell, U.Y., Corcuera, I., & Marti, A. (2013). Decelerated mass loss of Hurd and Johnsons Glaciers , Livingston Island , Antarctic Peninsula. *Journal of Glaciology*, *59*(213), 115–128. https://doi.org/10.3189/2013JoG12J144

Oliva, M., Navarro, F., Hrbáček, F., Hernández, A., Nývlt, D., Pereira, P., Ruiz-Fernández, J., & Trigo, R. (2017). Recent regional climate cooling on the Antarctic Peninsula and associated impacts on the cryosphere. *Science of The Total Environment*, *580*, 210–223. https://doi.org/10.1016/j.scitotenv.2016.12.030

Osmanoğlu, B., Braun, M., Hock, R., & Navarro, F.J. (2013). Surface velocity and ice discharge of the ice cap on King George Island, Antarctica. *Annals of Glaciology*, *54*(63), 111–119. https://doi.org/10.3189/2013AoG63A517

Paolo, F.S., Padman, L., Fricker, H.A., Adusumilli, S., Howard, S., & Siegfried, M.R. (2018). Response of Pacific-sector Antarctic ice shelves to the El Niño/Southern Oscillation. *Nature Geoscience*, *11*(2), 121–126. https://doi.org/10.1038/s41561-017-0033-0

Pętlicki, M., Sziło, J., MacDonell, S., Vivero, S., & Bialik, R.J. (2017). Recent deceleration of the ice elevation change of Ecology Glacier (King George Island, Antarctica). *Remote Sensing*, *9*(6), 7–9. https://doi.org/10.3390/rs9060520

Pudełko, R., Angiel, P.J., Potocki, M., Jędrejek, A., & Kozak, M. (2018). Fluctuation of glacial retreat rates in the eastern part of Warszawa icefield, King George Island, Antarctica, 1979-2018. *Remote Sensing*, *10*(6). https://doi.org/10.3390/rs10060892

Racoviteanu, A.E., Arnaud, Y., Williams, M.W., & Ordoñez, J. (2008). Decadal changes in glacier parameters in the Cordillera Blanca , Peru , derived from remote sensing. *Journal of Glaciology*, *54*(186), 499–510.

Rajat, S., Singh, B.R., Prakash, C., & Anita, S. (2022). Remote Sensing Applications : Society and Environment Glacier retreat in Himachal from 1994 to 2021 using deep learning. *Remote Sensing Applications: Society and Environment*, *28*, 100870. https://doi.org/10.1016/j.rsase.2022.100870

Rastner, P., Bolch, T., Mölg, N., Machguth, H., Bris, R. Le, & Paul, F. (2012). The first complete inventory of the local glaciers and ice caps on Greenland. *The Cryosphere*, *6*, 1483–1495. https://doi.org/10.5194/tc-6-1483-2012

Raup, B.H., Andreassen, L.M., Bolch, T., & Bevan, S. (2014). Remote sensing of glaciers. In *Remote Sensing of the Cryosphere* (pp. 123–156). https://doi.org/10.1002/9781118368909.ch7

RGI Consortium. (2017). Randolph Glacier Inventory – A Dataset of Global Glacier Outlines: Version 6.0 GLIMS Technical Report RGI. *Global Land Ice Measurements from Space, Colorado, USA. Digital Media*, *4*(July), 71.

Rückamp, M., & Blindow, N. (2012). King George Island ice cap geometry updated with airborne GPR measurements. *Earth System Science Data*, *4*(1), 23–30. https://doi.org/10.5194/essd-4-23-2012

Rückamp, M., Braun, M., Suckro, S., & Blindow, N. (2011). Observed glacial changes on the King George Island ice cap, Antarctica, in the last decade. *Global and Planetary Change*, *79*(1–2), 99–109. https://doi.org/10.1016/j.gloplacha.2011.06.009

Santamaría-del-Ángel, E., Cañon-Páez, M.-L., Sebastiá-Frasquet, M.-T., González-Silvera, A., Gutierrez, A.-L., Aguilar-Maldonado, J.-A., López-Calderón, J., Camacho-Ibar, V., Franco-Herrera, A., & Castillo-Ramírez, A. (2021). Interannual Climate Variability in the West Antarctic Peninsula under Austral Summer Conditions. *Remote Sensing*, *13*(6), 1122. https://doi.org/10.3390/rs13061122

Siegert, M., Atkinson, A., Banwell, A., Brandon, M., Convey, P., Davies, B., Downie, R., Edwards, T., Hubbard, B., Marshall, G., Rogelj, J., Rumble, J., Stroeve, J., & Vaughan, D. (2019). The Antarctic Peninsula under a 1.5°C global warming scenario. *Frontiers in Environmental Science*, *7*(JUN), 1–7. https://doi.org/10.3389/fenvs.2019.00102

Simões, J.C., Bremer, U.F., Aquino, F.E., & Ferron, F.A. (1999). Morphology and variations of glacial drainage basins in the King George Island ice field, Antarctica. *Annals of Glaciology*, *29*, 220–224. https://doi.org/10.3189/172756499781821085

Sobota, I., Araźny, A., & Kejna, M. (2015). Short-term mass changes and retreat of the Ecology and Sphinx glacier system , King George Island , Antarctic Peninsula. *Antarctic Science*, *May*. https://doi.org/10.1017/S0954102015000188

Turner, J., Lu, H., White, I., King, J.C., Phillips, T., Hosking, J.S., Bracegirdle, T.J., Marshall, G.J., Mulvaney, R., & Deb, P. (2016). Absence of 21st century warming on Antarctic Peninsula consistent with natural variability. *Nature*, *535*(7612), 411–415. https://doi.org/10.1038/nature18645

Turner, J., Marshall, G.J., Clem, K., Colwell, S., Phillips, T., & Lu, H. (2019). Antarctic temperature variability and change from station data. *International Journal of Climatology*, *40*(6), 2986–3007. https://doi.org/10.1002/joc.6378

Walker, C.C., & Gardner, A.S. (2017). Rapid drawdown of Antarctica's Wordie Ice Shelf glaciers in response to ENSO/Southern Annular Mode-driven warming in the Southern Ocean. *Earth and Planetary Science Letters*, *476*(November), 100–110. https://doi.org/10.1016/j.epsl.2017.08.005

Wei, T., Yan, Q., & Ding, M. (2019). Distribution and temporal trends of temperature extremes over Antarctica. *Environmental Research Letters*, *14*(8). https://doi.org/10.1088/1748-9326/ab33c1

Yao-Jun, L., Yong-Jian, D., Dong-Hui, S., & Rong-Jun, W. (2019). Regional differences in global glacier retreat from 1980 to 2015. *Advances in Climate Change Research*, *10*(4), 203–213. https://doi.org/10.1016/j.accre.2020.03.003

Yuan, X. (2004). ENSO-related impacts on Antarctic sea ice: A synthesis of phenomenon and mechanisms. *Antarctic Science*, *16*(4), 415–425. https://doi.org/10.1017/S0954102004002238

Zemp, M., & Welty, E. (2023). Temporal downscaling of glaciological mass balance using seasonal observations. *Journal of Glaciology*. https://doi.org/10.1017/ jog.2023.66